

Reconstructing the Noise Manifold for Image Denoising

Ioannis Marras¹, Grigorios G. Chrysos³, Ioannis Alexiou¹, Gregory Slabaugh^{1,2}, and Stefanos Zafeiriou³

¹Huawei Noah's Ark
²University College London
³Imperial College London

Abstract

Deep Convolutional Neural Networks (DCNNs) have been successfully used in many low-level vision problems such as image denoising, super-resolution etc. Although the conditional generative adversarial networks (cGAN) [45, 16] have led to large improvements in this task, there has been little effort in providing a cGAN with an explicit way of understanding the image noise for object-independent denoising reliable for real-world applications. The task of leveraging structures in the target space (clean image) of the cGAN is very unstable due to the complexity of patterns in natural scenes, so the presence of unnatural artifacts or over-smoothed image areas cannot be avoided. To fill the gap, in this work we introduce the idea of a cGAN which explicitly leverages structure in the image noise space. By using the residual learning in our model, the generator promotes the removal from the noisy image only that information which spans the manifold of the image noise. Based on our experiments, our model significantly outperforms existing state-of-the-art architectures.

1. Introduction

During image acquisition, due to the presence of noise some image corruption is inevitable and can degrade the visual quality considerably. Therefore, removing noise from the acquired image is a key step for many computer vision and image analysis applications [21]. Image denoising is the task of estimating the underlying clean image from its noisy observation. As an indispensable step in many digital imaging and computer vision systems, image denoising has been investigated for decades, while it is still an active research topic.

Denoising algorithms can be grouped in two categories: learning-based and model-based. Modelling the image prior

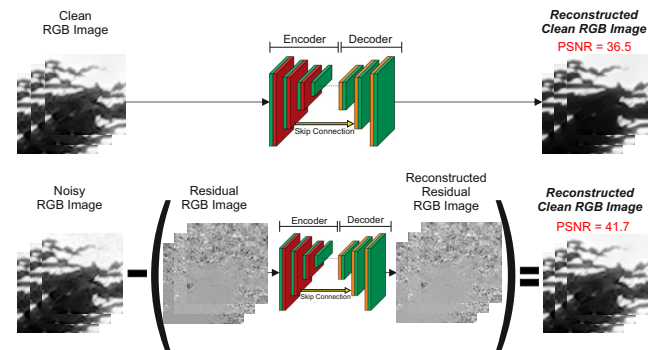


Figure 1: **Motivation of our method** (example in the RGB domain): By characterizing directly the image spatially variant noise, the reconstruction of the clean image is much more accurate. In this way of thinking, instead of constraining the output of a generator to span the target space, is better to constrain the generator to remove from the noisy image only that information which spans the manifold of the residual image.

from a set of noisy and ground-truth image sets is the goal of discriminative learning. The performance of the current learning models is limited by the inadequacy of the current methods to handle all possible levels of noise in a single model. In this category fall methods including brute force learning like MLP [10], deep convolutional neural networks (CNNs) [59, 60] or truncated inference [14]. On the other hand, the model-based algorithms are computationally expensive, time-consuming, unable to characterize complex image textures. In this category fall algorithms including external priors [7], Markov random field models [51, 54], gradient methods [56, 55], non-local self-similarity [34] and sparsity (e.g. MCWNNM [23]).

A denoising algorithm should be efficient, perform denoising using a single model and handle spatially variant noise when the noise standard-deviation is known or unknown. The physics of digital sensors and the steps of

an imaging pipeline are well-understood and can be leveraged to generate training data from almost any image using only basic information about the target camera sensor. Thus, recent work has shifted to sophisticated signal-dependent single source noise models, i.e. signal-dependent homoscedastic model [27], that better match the physics of image formation [39, 44, 8]. However, these models do not represent the spatial non-uniformity of noise power (e.g., fixed-pattern noise) or other sources of noise and nonlinearities [1], such as amplification noise and quantization [28]. Also, because of different camera sensors exhibit different noise characteristics, adapting a learned denoising algorithm to a new camera sensor may require capturing a new dataset. However, capturing noisy and noise-free image pairs is difficult, requiring long exposures or large bursts of images, and post-processing to combat camera motion and lighting changes.

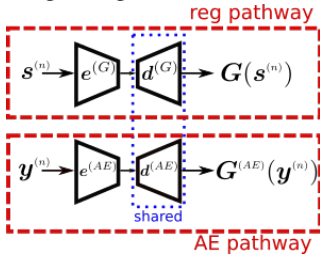


Figure 2: Schematic of the generator of RoCGAN (picture taken from [16]). The single pathway of the original cGAN model is replaced with two pathways.

In this paper, we introduce the idea of a conditional GAN which directly characterizes the image spatial variant noise for image denoising (Fig. 1). In RoCGAN [16], a combination of supervised (regression) and unsupervised (auto-encoder) ‘encoder-decoder’ type pathways applies implicit constraints in the latent subspaces. A schematic of the generator is illustrated in Fig. 2. The shared decoder is explicitly constrained to generate samples that span only the target manifold. The direct characterization of the target space greatly limits the denoising capability since the complexity of natural image patterns is extremely high. By adopting in our case the idea of residual learning in the regression pathway, the unsupervised pathway is forced to directly characterize the image noise. Intuitively, this can be thought of as constraining the regression pathway of our dense regression to *subtract from the noisy image only the residual that spans the image noise subspace*. This idea increases significantly the robustness of the model, makes easier the model adaptation to new camera sensors, while allows the combination in one model of many unsupervised pathways to deal with the case of image noise coming from more than one source. As in RoCGAN, the unsupervised pathway enables the utilization of all the samples in the target domain even in the absence of a corresponding input sample. Also,

the unsupervised pathway during inference is no longer required, therefore the testing complexity remains the same as in cGAN.

2. Related Work

In this section, we present the recent trends in image denoising. Image denoising has been the focus of a significant body of research in computer vision and image processing.

2.1. Image Prior Based Methods

Image prior based methods, e.g. NSCR [20], TWSC [57], WNNM [24], can be employed to solve the denoising problem of unknown noise because they do not require training data since they model the image prior over the noisy image directly. The classic internal statistics based method, BM3D [18], is based on the idea that natural images usually contain repeated patterns. It achieves impressive results by combining the non-local self-similarity model and sparse model. Similar image patterns are grouped together and jointly filtered. In contrast, Noise2Void (N2V) [35] and Noise2Noise (N2N) [38] do not require for training noisy image pairs, nor clean target images. N2N attempts to learn a mapping between pairs of independently degraded versions of the same training image. In method named *non-local means* (NLM) [9], the pixel values are predicted based on their noisy surroundings. Many variants of NLM and BM3D seeking self-similar patches in different transform domains were proposed e.g. SAPCA [34], NLB [36]. Sparsity is enforced by dictionary-based methods [19] by employing self-similar patches and learning over-complete dictionaries from clean images. For image patch restoration, maximum likelihood algorithms, e.g. the Gaussian Mixture Models (GMMs), were employed to learn a statistical priors from image patch groups [12, 58]. Dictionary learning based and basis-pursuit based algorithms such as KSVD [4] and Fields-of-Experts, such as TNRD [15], operated by finding image representations where sparsity holds or statistical regularities are well-modeled [62]. In [37], an extension of non-local Bayes approach, named NC, by modeling the noise of each patch group to be zero-mean correlated Gaussian distributed was proposed.

The disadvantage of this category of methods is that external information from possible many other images taken under the same condition with the image to be denoised cannot be used. Also in many cases, the computational cost at inference is very high. Furthermore, the generalization capabilities are limited because these methods are defined mostly based on human knowledge.

2.2. Discriminative Deep Learning Methods

In recent years, CNNs have achieved great success in many low-level vision problems, including image denois-

ing. The first attempt of employing CNNs for the regression task of image denoising was made in [30]. *Discriminative deep learning methods* are trained offline, extracting information from ground truth annotated training sets before they are applied to test data. In DnCNN [59] and IrCNN [60] networks, stacked convolution, batch normalization and ReLU layers used to estimate the residual [26] between the noisy input and the corresponding clean image. By adding symmetric skip connections, an improved encoder-decoder network for image denoising based on residual learning proposed in [42]. A densely connected denoising network, named Memnet, constructed in [53] to enable memory of the network. A multi-level wavelet CNN (MWCNN) model based on a U-Net architecture used in [41] to incorporate large receptive field for image denoising. By incorporating non-local operations into a recurrent neural network (RNN), a non-local recurrent network (NLRN) for image restoration presented in [40]. A network named N³Net [49] employs the k-nearest neighbor matching in the denoising network to exploit the non-local property of the image features. A fast and flexible network (FFDNet) which can process images with non-uniform noise corruption proposed in [61]. A residual in the residual structure (RIDNet) used in [6] to ease the flow of low-frequency information and apply feature attention to exploit the channel dependencies. Recently, a blind denoising model for real photographs named CBDNet [25] is composed of two subnetworks: noise estimation and non-blind denoising. It may require manual intervention to improve results. A self-guided network (SGN), which adopts a top-down self-guidance architecture to better exploit image multi-scale information presented in [22]. An image denoising network, named FOCNet [31], solves a fractional optimal control problem in a multi-scale approach. Although the methods in this category achieved high denoising quality, they cannot work in the absence of paired training data.

2.3. Generative Models

Generative adversarial networks (GANs) were recently trained to synthesize noise [13]. Since image noise is generated by the GAN-generator, pairs of corresponding clean and noisy images are obtained. These paired data are used for training CNNs. Also, Noise Flow [1] combines well-established basic parametric noise models (e.g. signal-dependent noise) with the flexibility and expressiveness of normalizing flow architectures to model noise distributions observed from large datasets of real noisy images. The flow model is conditioned on critical variables, such as intensity, camera type, and gain settings (i.e., ISO). However, it was not clear how to quantitatively assess the quality of the generated samples. To this end, there is still a lack of noise models that capture the characteristics of real noise.

3. Method

In this section, we introduce the system that we employ for the task of image denoising. The goal is to produce a single clean (RGB or RAW) image from a single noisy (RGB or RAW) image captured by a handheld camera. Firstly, we give a brief overview of the noise signal in real images (Section 3.1). Since our method extends the idea of RoCGAN method to an object-independent method, to make the paper self-contained we first review the original RoCGAN model (Section 3.2), before introducing our method (Section 3.3).

3.1. Image Noise Modeling

Camera sensors output RAW data in a linear color space, where pixel measurements are proportional to the number of photoelectrons collected. The primary sources of noise are shot noise, a Poisson process with variance equal to the signal level, and read noise, an approximately Gaussian process caused by a variety of sensor readout effects. These effects are well-modeled by a signal-dependent Gaussian distribution [27]:

$$x_p \sim \mathcal{N}(y_p, \sigma_r^2 + \sigma_s y_p) \quad (1)$$

where x_p is a noisy measurement of the true intensity y_p at pixel p . The noise parameters σ_r and σ_s are fixed for each image but can vary from image to image as sensor gain (ISO) changes.

However, the noise in real images comes from various sources (dark current noise, thermal noise, etc.), and is much more sophisticated [47]. Although the noise in RAW sensor data is well understood, in the RGB domain the case of losing signal due to the post-processing performed between capture and display (e.g., demosaicking, sharpening, tone mapping, and compression) cannot be avoided which makes the image denoising task more challenging. For example, by taking in-camera image processing pipeline into account, the channel-independent noise assumption may not hold true, and several approaches [32, 46] were proposed for cross-channel noise modeling. In general, a realistic noise model as well as the in-camera image processing pipeline are important aspects in training CNN-based denoising methods for real photographs [25, 6].

3.2. Robust Conditional GAN

The GAN consists of a generator and a discriminator module commonly optimized with alternating gradient descent methods. The generator samples z from a prior distribution p_z , e.g. uniform, and tries to model the target distribution p_d ; the discriminator D tries to distinguish between the samples generated from the model and the target (ground-truth) distributions. Conditional GAN (cGAN) [45] extend the formulation by providing the generator with additional labels. In cGAN, the generator G typically takes the form of an encoder-decoder network where

the encoder projects the label into a low-dimensional latent subspace and the decoder performs the opposite mapping, i.e. from low-dimensional to high-dimensional subspace. If we denote \mathbf{s} the conditioning label and \mathbf{y} a sample from the target distribution, the adversarial loss is expressed as:

$$\mathcal{L}_{adv}(\mathbf{G}, \mathbf{D}) = \mathbb{E}_{\mathbf{s}, \mathbf{y} \sim p_d(\mathbf{s}, \mathbf{y})} [\log \mathbf{D}(\mathbf{y}|\mathbf{s})] + \mathbb{E}_{\mathbf{s} \sim p_d(\mathbf{s}), \mathbf{z} \sim p_z(\mathbf{z})} [\log(1 - \mathbf{D}(\mathbf{G}(\mathbf{s}, \mathbf{z})|\mathbf{s}))] \quad (2)$$

by solving the following min-max problem:

$$\min_{\mathbf{w}_G} \max_{\mathbf{w}_D} \mathcal{L}_{adv}(\mathbf{G}, \mathbf{D}) = \min_{\mathbf{w}_G} \max_{\mathbf{w}_D} \mathbb{E}_{\mathbf{s}, \mathbf{y} \sim p_d(\mathbf{s}, \mathbf{y})} [\log \mathbf{D}(\mathbf{y}|\mathbf{s}, \mathbf{w}_D)] + \mathbb{E}_{\mathbf{s} \sim p_d(\mathbf{s}), \mathbf{z} \sim p_z(\mathbf{z})} [\log(1 - \mathbf{D}(\mathbf{G}(\mathbf{s}, \mathbf{z}|\mathbf{w}_G)|\mathbf{s}, \mathbf{w}_D))] \quad (3)$$

where $\mathbf{w}_G, \mathbf{w}_D$ denote the generator’s and the discriminator’s parameters respectively. To simplify the notation, we drop the dependencies on the parameters and the noise \mathbf{z} in the rest of the paper.

RoCGAN, like cGAN, was successfully applied in the past for the task of image denoising. Both cGAN and RoCGAN consist of a generator and a discriminator (Fig. 2). The generator of RoCGAN includes two pathways instead of the single pathway of the original cGAN. The first pathway, referred as *reg pathway* henceforth, performs a similar regression (denoising) as its counterpart in cGAN. It accepts a sample from the source domain (noisy image) and maps it to the target domain (clean image). RoCGAN introduced an additional unsupervised pathway, named *AE pathway* which works as an autoencoder in the target domain. Both pathways consist of the same encoder-decoder networks. By sharing the weights of their decoders, RoCGAN promotes the regression outputs to span the target manifold and not induce arbitrarily large errors. The discriminator remains the same as the cGAN.

The *AE pathway* contributes the following loss term:

$$\mathcal{L}_{AE} = \sum_{n=1}^N [f_d(\mathbf{y}^{(n)}, \mathbf{G}^{(AE)}(\mathbf{y}^{(n)}))], \quad (3)$$

where f_d denotes a divergence metric (ℓ_1 loss), the superscript ‘AE’ abbreviates modules of the AE pathway, ‘G’ modules of the reg pathway and $\mathbf{G}^{(AE)}(\mathbf{y}^{(n)}) = \mathbf{d}^{(AE)}(\mathbf{e}^{(AE)}(\mathbf{y}^{(n)}))$ is the output of the AE pathway.

Despite sharing the weights of the decoders, RoCGAN forced the latent representations of the two pathways to span the same space. To further reduce the distance of the two representations in the latent space, a latent loss term \mathcal{L}_{lat} used. This term minimizes the distance between the encoders’ outputs, i.e. the two representations are spatially close (in the subspace spanned by the encoders). The latent loss term is:

$$\mathcal{L}_{lat} = \sum_{n=1}^N \|e^{(G)}(\mathbf{s}^{(n)}) - e^{(AE)}(\mathbf{y}^{(n)})\|. \quad (4)$$

The feature matching loss [52, 29] enables the network to match the data and the model’s distribution faster. RoCGAN considers this as part of the vanilla cGAN. The intuition is that to match the high-dimensional distribution of the data with *reg pathway*, their projections in lower-dimensional spaces are encouraged to be similar. The feature matching loss is:

$$\mathcal{L}_f = \sum_{n=1}^N \|\pi(\mathbf{G}(\mathbf{s}^{(n)})) - \pi(\mathbf{y}^{(n)})\|, \quad (5)$$

where $\pi(\cdot)$ extracts the features from the penultimate layer of the discriminator.

Skip connections can enable deeper layers to capture more abstract representations without the need of memorizing all the information. The lower-level representations are propagated directly to the decoder through the shortcut, which makes it harder to train the longer path [50], i.e. the network excluding the skip connections. This challenge is implicitly tackled by maximizing the variance captured by the longer path representations. The Decov loss term [17] that penalizes the correlations in the representations (of a layer) and thus implicitly encourages the representations to capture diverse and useful information is used. This loss may be applied to a single layer or multiple layers in a network, while for the j^{th} layer this loss is defined as:

$$\mathcal{L}_{decov}^j = \frac{1}{2} (\|\mathbf{C}^j\|_F^2 - \|\text{diag}(\mathbf{C}^j)\|_2^2) \quad (6)$$

where $\text{diag}(\cdot)$ computes the diagonal elements of a matrix and \mathbf{C}^j is the covariance matrix of the j^{th} layer’s representations. The loss is minimized when the covariance matrix is diagonal, i.e. it imposes a cost to minimize the covariance of hidden units without restricting the diagonal elements that include the variance of the hidden representations.

By defining as $\mathbf{G}(\mathbf{s}^{(n)}) = \mathbf{d}^{(G)}(\mathbf{e}^{(G)}(\mathbf{s}^{(n)}))$ the output of the reg pathway, the final loss function of RoCGAN combines the loss terms of the original cGAN with the additional three terms for the AE pathway:

$$\mathcal{L}_{RoCGAN} = \mathcal{L}_{adv} + \underbrace{\lambda_c \cdot \sum_{n=1}^N \|\mathbf{G}(\mathbf{s}^{(n)}) - \mathbf{y}^{(n)}\|}_{\text{content-loss}} + \underbrace{\lambda_\pi \cdot \mathcal{L}_f}_{\text{cGAN-loss}} + \lambda_{ae} \cdot \mathcal{L}_{AE} + \lambda_l \cdot \mathcal{L}_{lat} + \lambda_d \cdot \sum_j \mathcal{L}_{decov}^j \quad (7)$$

where $\lambda_c, \lambda_\pi, \lambda_{ae}, \lambda_l$ and λ_d are hyper-parameters to balance the loss terms.

3.3. Image denoising based on noise manifold reconstruction

There are two major drawbacks of the RoCGAN method related to the use of skip connections or not. In the absence

of skip connections, RoCGAN performs well only in the case of object-dependent image denoising (i.e. face denoising). This restricts its use since the need of having different models for different objects makes it unsuitable for digital devices with limited resources (e.g. smartphones) where the run-time performance is of importance.

The *AE pathway*, is an unsupervised learning method whose (hidden) layers contain representations of the input data sufficiently powerful for compressing (and decompressing) the data while losing as little information as possible. However, even in the presence of skip connections the *AE pathway* is not capable of reconstructing all natural scenes and patterns. Therefore, the use of one auto-encoder to define a nonlinear manifold which can accurately reconstruct image patterns from a variety of real complex objects/scenes is not realistic. As a result, RoCGAN very often hallucinates complex image structures by introducing severe blurry effects or unusual image patterns/artifacts.

To tackle the problems mentioned above, the proposed method introduces the idea of directly reconstructing the image noise. Just like RoCGAN, our method consists of a generator and a discriminator. Similarly, the generator includes two pathways with similar type of architectures. Rather than directly outputting the denoised image, like in RoCGAN, the first pathway in our method is designed to predict the ground-truth residual image, i.e., the difference between the noisy observation s and the clean (ground-truth) image y , $v = s - y$. This residual learning can be benefit from any conditional information related to the camera sensor noise characteristics, c , which is explicitly given to the generator in concatenation (denoted as \frown) with s to get its output $G'(s \frown c)$. In other words, the proposed conditional *reg pathway* implicitly removes the latent clean image with the operations in the hidden layers. Because of that, the unsupervised pathway works as a conditional auto-encoder in the domain of v . The input to this pathway is v in concatenation with y and c . In that way, by giving explicitly y as additional input, the task of the *AE pathway* is not to learn the underlying structure of a huge variety of complex image patterns, but to learn how image structures are affected by the presence of structured noise. By sharing the weights of their decoders, the generator adopts the residual learning strategy to remove from the noisy observation that image information which spans the image noise manifold. Two Unet style skip connections from the encode to the decoder are added enforcing our method to learn the residual between the features corresponding to the image and to the residual image structures.

In the case of image denoising in RGB domain, the images are 3-channel based tensors. On the other hand in RAW domain, each pixel in a conventional camera sensor (linear Bayer sensor readings) is covered by a single red, green, or blue color filter, arranged in a Bayer pattern, such

as R-G-G-B. Also, the information that c represents varies. In the case the camera noise model is known, c could contain the two noise parameters σ_r and σ_s (both same for each pixel) as described in Section 3.1. In the case of more than one camera sensor, c could also contain one hot vector per pixel defining the camera id used to take each picture.

Noising is a challenging process to be reversed by the few convolutional layers of the encoder in *reg pathway* especially in the object-independent scenario. To that end, a backbone network is used prior to *reg pathway* to extract complex feature representations useful to preserve later on the low and high image frequencies. The backbone is a residual network (ResNet) created by stacking a few building blocks introduced in [26]) A schematic of the proposed generator is illustrated in Fig. 3. The discriminator (Fig. 4a) remains the same as the RoCGAN. It accepts the predicted clean image, $s - G'(s \frown c)$, along with y as input.

In our method, the content loss consists of two terms that compute the per-pixel difference between the predicted clean image, and the clean (ground-truth) image. The two terms are i) the ℓ_1 loss between the ground-truth image and the output of the generator, ii) the ℓ_1 of their gradients; mathematically expressed as:

$$\mathcal{L}'_c = \lambda_c \| (s^{(n)} - G'(s^{(n)} \frown c^{(n)})) - y^{(n)} \|_{\ell_1} + \lambda_{cg} \| \nabla (s^{(n)} - G'(s^{(n)} \frown c^{(n)})) - \nabla y^{(n)} \|_{\ell_1}. \quad (8)$$

The loss term for the unsupervised module becomes:

$$\mathcal{L}'_{AE} = \sum_{n=1}^N [f_d(v^{(n)}, G'^{(AE)}(v^{(n)} \frown y^{(n)} \frown c^{(n)}))] \quad (9)$$

where $G'^{(AE)}(v^{(n)} \frown y^{(n)} \frown c^{(n)}) = d^{(AE)}(e^{(AE)}(v^{(n)} \frown y^{(n)} \frown c^{(n)}))$ is the output of the AE pathway and f_d represents an ℓ_2 loss due to the auto-encoder in the in the domain of the residual image. The latent loss term becomes:

$$\mathcal{L}'_{lat} = \sum_{n=1}^N \| e^{(G)}(s^{(n)} \frown c^{(n)}) - e^{(AE)}(v^{(n)} \frown y^{(n)} \frown c^{(n)}) \| \quad (10)$$

and the feature matching loss becomes:

$$\mathcal{L}'_f = \sum_{n=1}^N \| \pi(s^{(n)} - G'(s^{(n)} \frown c^{(n)})) - \pi(y^{(n)}) \|. \quad (11)$$

The final loss function of our method is:

$$\mathcal{L}_{ours} = \mathcal{L}_{adv} + \mathcal{L}'_c + \lambda_\pi \cdot \mathcal{L}'_f + \lambda_{ae} \cdot \mathcal{L}'_{AE} + \lambda_l \cdot \mathcal{L}'_{lat} + \lambda_d \cdot \sum_j \mathcal{L}'_{decov}^j \quad (12)$$

where $\lambda_c, \lambda_{cg}, \lambda_\pi, \lambda_{ae}, \lambda_l$ and λ_d are hyper-parameters to balance the loss terms.

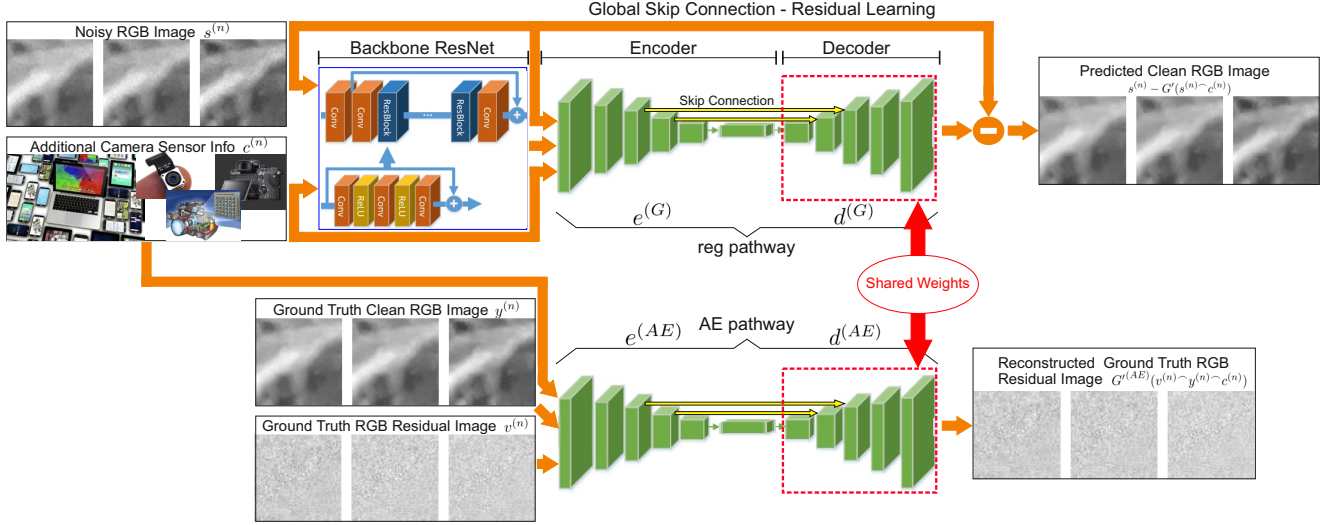


Figure 3: Schematic of the generator of our method (example in the RGB domain).



Figure 4: (a) The discriminator in our method remains the same as the cCGAN (example in the RGB domain). (b) In the case of camera multi-source image noise, more than one *AE pathway* can be employed. Each pathway is responsible for removing noise structure that comes from a specific noise source.

The design of our generator has many advantages over RoCGAN’s generator:

- For the *AE pathway*, the reconstruction of v is an easier task comparing to the reconstruction of y . In other words, we can learn how to turn bad images into good images by only looking at the structure of the residual image. This property: i) makes our method an object-independent image denoiser and ii) helps the denoiser largely avoid the image over-smoothing, something essential for any image denoiser.
- The *AE pathway* enables the utilization of all the samples in the domain of the residual image even in the absence of the corresponding noisy input samples. For example, in the case of a well defined image noise source, like the one described in Section 3.1, a huge amount of different residual image realizations (e.g. based on different ISO values) could be generated and used to train that pathway.
- In the case of camera multi-source image noise, more than one *AE pathway* can be employed (Fig. 4b). Each pathway is responsible for removing noise information that comes from a specific noise source.
- It is easier to adapt an existing trained model to a new camera sensor. To do so, the *AE pathway* must be re-trained from scratch while the *reg pathway* needs only to be fine-tuned using a small number of paired training samples obtained using the new sensor.
- According to [26], when the original mapping (as in RoCGAN) is more like an identity mapping, the residual mapping will be much easier to be optimized. Note that y is much more like s than $G'(s^{(n)} \frown c^{(n)})$ (especially when the noise level is low). Thus, the original mapping would be closer to an identity mapping than $G'(s^{(n)} \frown c^{(n)})$, and the residual learning formulation is more suitable for image denoising [59] because it allows the training of a single CNN for denoising of

images corrupted by a wide range of noise levels.

4. Experiments

4.1. Training Settings

Synthetic noisy images can be combined with real noisy data to improve the generalization ability of our method to real photographs. To generate them, we follow the same pipeline used in [25] which is based on the noise model described in Section 3.1. To do so, we employ BSD500 [43], DIV2K [3], and MIT-Adobe FiveK [11], resulting in 3.5K images while for real noisy images, we extract cropped patches of 512×512 from SSID [2] and RENOIR [5]. Finally, the data augmentation procedure results in with 64×64 image patches. In our ‘*encoder-decoder*’ architecture (same for both pathways) 11 layers are used with an latent space of dimensions $MB \times 2 \times 2 \times 1024$, where MB stands for the mini-batch size.

In the backbone network, three building blocks used with the default parameters as in [26]. As in RocGAN, the Decov loss is applied in the output of the encoder minimizing the correlations in the longer path. The values of the additional hyper-parameters are $\lambda_{ae} = 10$, $\lambda_{cg} = 0.45$, $\lambda_l = 0.1$ and $\lambda_d = 1$. The common hyper-parameters λ_π and λ_c with the vanilla cGAN remain the same. For both pathways: the kernel size used is 3×3 ; Adam [33] is used as the optimizer with default parameters; the learning rate is initially set to 10^{-3} and then halved after 10^6 iterations; ReLU activation used; the network ran for 35 epochs. Our method is implemented in the TensorFlow framework and trained with a single NVIDIA GeForce GTX 1080Ti GPU.

4.2. Comparisons

To assess the performance of our method, we used public datasets that significantly improve upon earlier (and often unrealistic) benchmarks for denoising.

Evaluation on Darmstadt Noise Dataset (DnD) [48] : DnD is a novel benchmark dataset which consists of realistic uncompressed photos from 50 scenes taken by 4 different standard consumer cameras of natural “in the wild” scene content. In DnD: the camera metadata has been captured; the noise properties have been carefully calibrated; and the image intensities are presented as RAW unprocessed linear intensities. For each real high-resolution image, the noisy high-ISO image is paired with the corresponding (nearly) noise-free low-ISO ground-truth image.

The evaluation of DnD is separated in two categories: algorithms that use linear Bayer sensor readings or algorithms that use bilinearly demosaiced sRGB images as input. Thus, PSNR and SSIM for each technique are reported on RAW and sRGB outputs. The quantitative results on the DnD benchmark with respect to prior work is shown in Table 1. For algorithms which have been evaluated with and with-

Algorithm	Type	RAW		sRGB		Runtime (ms)
		PSNR	SSIM	PSNR	SSIM	
FoE [51]	Non-blind	45.78	0.9666	35.99	0.9042	-
TNRD [15] + VST	Non-blind	45.70	0.9609	36.09	0.8883	5,200
MLP [10] + VST	Non-blind	45.71	0.9629	36.72	0.9122	~60,000
MCWNNM [23]	Non-blind	-	-	37.38	0.9294	208,100
EPLL [62] + VST	Non-blind	46.86	0.9730	37.46	0.9245	-
KSVD [4] + VST	Non-blind	46.87	0.9723	37.63	0.9287	>60,000
WNNM [24] + VST	Non-blind	47.05	0.9722	37.69	0.9260	-
NCSR [20] + VST	Non-blind	47.07	0.9688	37.79	0.9233	-
BM3D [18] + VST	Non-blind	47.15	0.9737	37.86	0.9296	6,900
TWSC [57]	Blind	-	-	37.94	0.9403	195,200
CBDNet [25]	Blind	-	-	38.06	0.9421	400
DnCNN [59]	Blind	47.37	0.9760	38.08	0.9357	60
N ³ Net [49]	Blind	47.56	0.9767	38.32	0.9384	210
RIDNet [6]	Blind	-	-	39.23	0.9526	215
UPI [8]	Blind	48.89	0.9824	40.35	0.9641	22
Ours (empty <i>c</i>)	Blind	49.09	0.9829	40.54	0.9657	52
Ours (Non empty <i>c</i>)	Non-Blind	49.45	0.9847	40.84	0.9679	63

Table 1: The quantitative results on the DnD benchmark.

out a variance stabilizing transformation (VST), the version which performs better is reported. For completeness, the evaluation of algorithms that only operate on sRGB inputs is also reported. The two variants of our model (one targeting sRGB and the other targeting RAW) produce significantly higher PSNRs and SSIMs than all baseline techniques across all outputs, with each model variant outperforming the other for the domain that it targets. For each variant, a blind and a non-blind version of our method had been tested based on the info that *c* represents. The blind version uses no extra conditional information along with the noisy input image. As described in Section 3.3, in the non-blind version, *c* could contain information regarding the camera noise model (signal-dependent noise variance) and/or the camera id. Runtimes (mean over 100 runs) reported in bibliography are presented as well in Table 1. In addition, some qualitative results are given in Fig. 5. The runtime of our blind model is 52ms while for the non-blind one is 63ms given as input 512×512 images. The time taken for data to be transferred to the GPU is excluded.

Evaluation on Nam Dataset [46]: Nam dataset consists of 11 static scenes captured by 3 consumer cameras. For each scene, 500 JPEG noisy temporal images were captured to compute the temporal nearly noise-free mean image and covariance matrix for each pixel. The quantitative results on the Nam benchmark with respect to prior work is shown in Table 2. Both the blind and non-blind version of our method are evaluated. In addition, some qualitative results are given in Fig. 6. Our model produces significantly higher PSNR and SSIM than all baseline techniques. The noisy images are JPEG compressed, thus our model tries to specifically deal with the JPEG compression.

Evaluation on Smartphone Image Denoising Dataset (SIDD) [2]: SSID is real noise dataset which a large number of available test (validation) images. The quantitative results on the SIDD benchmark with respect to prior work is shown in Table 3. Both the blind and non-blind version of

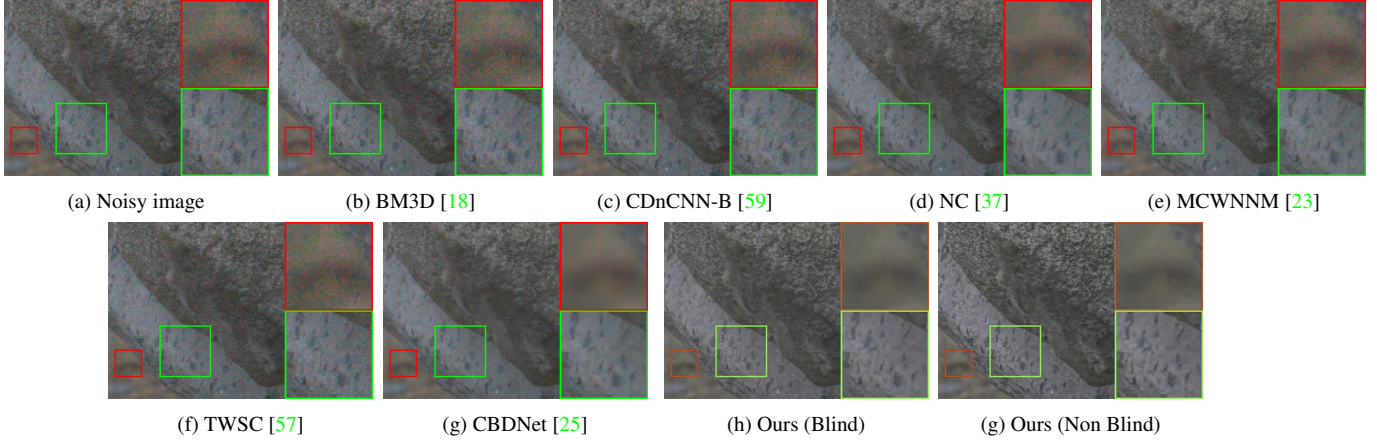


Figure 5: Example of image denoising of a DnD image.

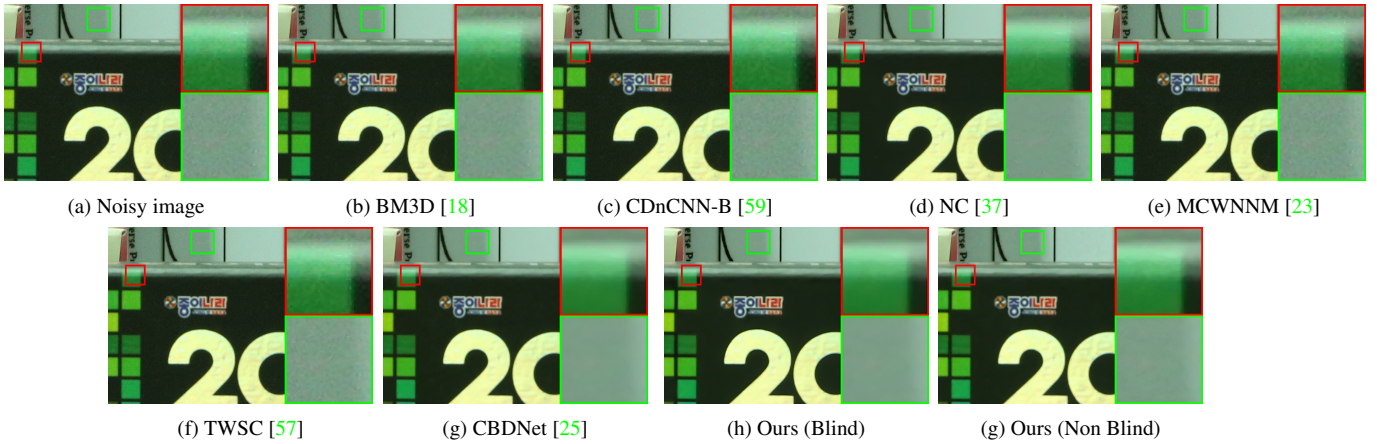


Figure 6: Example of image denoising of a Nam image.

Method	Type	PSNR	SSIM
CDnCNN-B [59]	Blind	37.49	0.9272
TWSC [57]	Blind	37.52	0.9292
MCWNNM [23]	Blind	37.91	0.9322
BM3D [18]	Non-blind	39.84	0.9657
NC [37]	Blind	40.41	0.9731
WNNM [24]	Non-blind	41.04	0.9768
CBDNet-JPEG [25]	Blind	41.31	0.9784
Ours (empty c)	Blind	41.52	0.9795
Ours (Non empty c)	Non-Blind	41.88	0.9822

Table 2: The quantitative results on the Nam dataset.

Method	Type	PSNR
DnCNN-B [59]	Blind	26.21
FFDNet [61]	Blind	29.20
CBDNet-JPEG [25]	Blind	30.78
BM3D [18]	Non-blind	30.88
RIDNet [6]	Blind	38.71
Ours (empty c)	Blind	39.00
Ours (Non empty c)	Non-Blind	39.69

Table 3: The quantitative results on the SIDD.

our method are evaluated. Our model produces significantly higher PSNR than all baseline techniques.

Based on all our experiments, our method better restores the true colors which are closer to the original pixel values than the competing methods. Also, by directly characterizing the image noise our method avoids in great degree the image over-smoothing.

5. Conclusions

In this work, we show that is easier to turn noisy images into clean images only by looking at the structure of the residual image. We introduce the idea of a cGAN which explicitly leverages structure in the image noise space of the model. In that case, the generator, by adopting the residual learning, promotes the removal from the noisy image only that information which spans the manifold of the image noise. Our model significantly outperforms existing state-

of-the-art architectures.

References

- [1] A. Abdelhamed, M. A. Brubaker, and M. S. Brown. Noise flow: Noise modeling with conditional normalizing flows. *ArXiv*, 2019. 2, 3
- [2] A. Abdelhamed, S. Lin, and M. S. Brown. A high-quality denoising dataset for smartphone cameras. In *IEEE Conference on Computer Vision and Pattern Recognition (CVPR)*, 2018. 7
- [3] E. Agustsson and R. Timofte. Ntire 2017 challenge on single image super-resolution: Dataset and study. pages 1122–1131, 2017. 7
- [4] M. Aharon, M. Elad, and A. Bruckstein. K-SVD: An algorithm for designing overcomplete dictionaries for sparse representation. *IEEE Transactions on Signal Processing (TSP)*, 54:4311 – 4322, 2006. 2, 7
- [5] J. Anaya and A. Barbu. Renoir - a dataset for real low-light noise image reduction. *Journal of Visual Communication and Image Representation*, 51:144–154, 2018. 7
- [6] S. Anwar and N. Barnes. Real image denoising with feature attention. In *IEEE International Conference on Computer Vision (ICCV)*, 2019. 3, 7, 8
- [7] S. Anwar, F. Porikli, and C. P. Huynh. Category-specific object image denoising. *IEEE Transactions on Image Processing*, 26(11):5506–5518, 2017. 1
- [8] T. Brooks, B. Mildenhall, T. Xue, J. Chen, D. Sharlet, and J. T. Barron. Unprocessing images for learned raw denoising. *IEEE Conference on Computer Vision and Pattern Recognition (CVPR)*, 2019. 2, 7
- [9] A. Buades, B. Coll, and J. M. Morel. A non-local algorithm for image denoising. In *IEEE Conference on Computer Vision and Pattern Recognition (CVPR)*, pages 60–65, 2005. 2
- [10] H. C. Burger, C. J. Schuler, and S. Harmeling. Image denoising: Can plain neural networks compete with bm3d? pages 2392–2399, 2012. 1, 7
- [11] V. Bychkovsky, S. Paris, E. Chan, and F. Durand. Learning photographic global tonal adjustment with a database of input / output image pairs. In *The Twenty-Fourth IEEE Conference on Computer Vision and Pattern Recognition*, 2011. 7
- [12] F. Chen, L. Zhang, and H. Yu. External patch prior guided internal clustering for image denoising. In *IEEE International Conference on Computer Vision (ICCV)*, pages 603–611, 2015. 2
- [13] J. Chen, J. Chen, H. Chao, and M. Yang. Image blind denoising with generative adversarial network based noise modeling. In *IEEE Conference on Computer Vision and Pattern Recognition (CVPR)*, 2018. 3
- [14] Y. Chen and T. Pock. Trainable nonlinear reaction diffusion: A flexible framework for fast and effective image restoration. *IEEE Transactions on Pattern Analysis and Machine Intelligence*, 39:1–1, 08 2016. 1
- [15] Y. Chen, W. Yu, and T. Pock. On learning optimized reaction diffusion processes for effective image restoration. *IEEE Conference on Computer Vision and Pattern Recognition (CVPR)*, 2015. 2, 7
- [16] G. G. Chrysos, J. Kossaifi, and S. Zafeiriou. Robust conditional generative adversarial networks. In *International Conference on Learning Representations (ICLR)*, 2019. 1, 2
- [17] M. Cogswell, F. Ahmed, R. Girshick, L. Zitnick, and D. Batra. Reducing overfitting in deep networks by decorrelating representations. In *International Conference on Learning Representations (ICLR)*, 2016. 4
- [18] K. Dabov, A. Foi, V. Katkovnik, and K. Egiazarian. Image denoising by sparse 3-D transform-domain collaborative filtering. *IEEE Transactions on image processing*, 16(8):2080–2095, 2007. 2, 7, 8
- [19] W. Dong, X. Li, L. Zhang, and G. Shi. Sparsity-based image denoising via dictionary learning and structural clustering. In *IEEE Conference on Computer Vision and Pattern Recognition (CVPR)*, pages 674–697, 2011. 2
- [20] W. Dong, L. Zhang, G. Shi, and X. Li. Nonlocally centralized sparse representation for image restoration. *IEEE Transactions on Image Processing*, 22:1620–1630, 2013. 2, 7
- [21] R.C. Gonzalez. *Digital Image Processing 2Nd Ed.* Prentice-Hall Of India Pvt. Limited, 2002. 1
- [22] S. Gu, Y. Li, L. V. Gool, and R. Timofte. Self-guided network for fast image denoising. In *IEEE International Conference on Computer Vision (ICCV)*, 2019. 3
- [23] S. Gu, L. Zhang, W. Zuo, and X. Feng. Weighted nuclear norm minimization with application to image denoising. *IEEE Conference on Computer Vision and Pattern Recognition*, pages 2862–2869, 2014. 1, 7, 8
- [24] S. Gu, L. Zhang, W. Zuo, and X. Feng. Weighted nuclear norm minimization with application to image denoising. In *IEEE Conference on Computer Vision and Pattern Recognition (CVPR)*, 2014. 2, 7, 8
- [25] S. Guo, Z. Yan, K. Zhang, W. Zuo, and L. Zhang. Toward convolutional blind denoising of real photographs. *2019 IEEE Conference on Computer Vision and Pattern Recognition (CVPR)*, 2019. 3, 7, 8
- [26] K. He, X. Zhang, S. Ren, and J. Sun. Deep residual learning for image recognition. In *IEEE Conference on Computer Vision and Pattern Recognition (CVPR)*, pages 770–778, 2016. 3, 5, 6, 7
- [27] G. Healey and R. Kondepudy. Radiometric ccd camera calibration and noise estimation. *IEEE Trans. Pattern Anal. Mach. Intell.*, 16:267–276, 1994. 2, 3
- [28] G. C. Holst. *CCD Arrays, Cameras, and Displays.* SPIE Optical Engineering Press, second edition, 1998. 2
- [29] P. Isola, J. Y. Zhu, T. Zhou, and A. A. Efros. Image-to-image translation with conditional adversarial networks. In *CVPR*, 2017. 4
- [30] V. Jain and S. Sebastian. Natural image denoising with convolutional networks. In *Advances in Neural Information Processing Systems*, pages 769–776, 2009. 2
- [31] X. Jia, S. Liu, X. Feng, and L. Zhang. Focnet: A fractional optimal control network for image denoising. In *IEEE Conference on Computer Vision and Pattern Recognition (CVPR)*, 2019. 3

- [32] S. J. Kim, H. T. Lin, Z. Lu, S. Süsstrunk, S. Lin, and M. S. Brown. A new in-camera imaging model for color computer vision and its application. *IEEE Transactions on Pattern Analysis and Machine Intelligence*, 34:2289–2302, 2012. 3
- [33] D. P. Kingma and J. Ba. Adam: A method for stochastic optimization. *arXiv preprint arXiv:1412.6980*, 2014. 7
- [34] K. Kostadin, A. Foi, V. Katkovnik, and K. Egiazarian. BM3D image denoising with shape-adaptive principal component analysis. 2009. 1, 2
- [35] A. Krull, T. O. Buchholz, and F. Jug. Noise2void - learning denoising from single noisy images. In *IEEE Conference on Computer Vision and Pattern Recognition (CVPR)*, 2018. 2
- [36] M. Lebrun, A. Buades, and J. M. Morel. A nonlocal bayesian image denoising algorithm. *SIAM Journal on Imaging Sciences*, 6:1665–1688, 2013. 2
- [37] M. Lebrun, M. Colom, and J. M. Morel. The noise clinic: a blind image denoising algorithm. *Image Processing On Line (IPOL)*, 5:1–54, 2015. 2, 8
- [38] J. Lehtinen, J. Munkberg, J. Hasselgren, S. Laine, T. Karras, M. Aittala, and T. Aila. Noise2Noise: Learning image restoration without clean data. In *International Conference on Machine Learning (ICML)*, pages 2965–2974, 2018. 2
- [39] C. Liu, R. Szeliski, S. B. Kang, C. L. Zitnick, and W. T. Freeman. Automatic estimation and removal of noise from a single image. *IEEE Transactions on Pattern Analysis and Machine Intelligence*, 30:299–314, 2008. 2
- [40] D. Liu, B. Wen, Y. Fan, C. Loy, and T. S. Huang. Non-local recurrent network for image restoration. In *International Conference on Neural Information Processing Systems (NIPS)*, pages 1680–1689, 2018. 3
- [41] P. Liu, H. Zhang, K. Zhang, L. Lin, and W. Zuog. Multi-level wavelet-cnn for image restoration. In *IEEE Conference on Computer Vision and Pattern Recognition (CVPR)*, page 773782, 2018. 3
- [42] X. Mao, C. Shen, and Y. B. Yang. Image restoration using very deep convolutional encoder-decoder networks with symmetric skip connections. In *Advances in Neural Information Processing Systems*, pages 2802–2810, 2016. 3
- [43] D. Martin, C. Fowlkes, D. Tal, and J. Malik. A database of human segmented natural images and its application to evaluating segmentation algorithms and measuring ecological statistics. In *IEEE International Conference on Computer Vision (ICCV)*, volume 2, pages 416–423, July 2001. 7
- [44] B. Mildenhall, J. T. Barron, J. Chen, D. Sharlet, R. Ng, and R. Carroll. Burst Denoising With Kernel Prediction Networks. In *The IEEE Conference on Computer Vision and Pattern Recognition (CVPR)*, June 2018. 2
- [45] M. Mirza and S. Osindero. Conditional generative adversarial nets. *arXiv preprint arXiv:1411.1784*, 2014. 1, 3
- [46] S. Nam, Y. Hwang, Y. Matsushita, and S. J. Kim. A holistic approach to cross-channel image noise modeling and its application to image denoising. *IEEE Conference on Computer Vision and Pattern Recognition (CVPR)*, pages 1683–1691, 2016. 3, 7
- [47] Alberto Ortiz and Gabriel Oliver. Radiometric calibration of ccd sensors: dark current and fixed pattern noise estimation. *IEEE International Conference on Robotics and Automation*, 2004. *Proceedings. ICRA '04. 2004*, 5:4730–4735 Vol.5, 2004. 3
- [48] T. Plotz and S. Roth. Benchmarking denoising algorithms with real photographs. *IEEE Conference on Computer Vision and Pattern Recognition (CVPR)*, pages 2750–2759, 2017. 7
- [49] T. Plötz and S. Roth. Neural nearest neighbors networks. In *Advances in Neural Information Processing Systems (NeurIPS)*, 2018. 3, 7
- [50] A. Rasmus, M. Berglund, M. Honkala, H. Valpola, and T. Raiko. Semi-supervised learning with ladder networks. In *International Conference on Neural Information Processing Systems (NIPS)*, pages 3546–3554, 2015. 4
- [51] S. Roth and M. J. Black. Fields of experts. *International Journal of Computer Vision*, 82(2):205–229, 2009. 1, 7
- [52] T. Salimans, I. Goodfellow, W. Zaremba, V. Cheung, A. Radford, and X. Chen. Improved techniques for training gans. In *International Conference on Neural Information Processing Systems (NIPS)*, pages 2234–2242, 2016. 4
- [53] Y. Tai, J. Yang, X. Liu, and C. Xu. Memnet: A persistent memory network for image restoration. In *IEEE International Conference on Computer Vision (ICCV)*, pages 4549–4557, 2017. 3
- [54] M. F. Tappen, C. Liu, E. H. Adelson, and W. T. Freeman. Learning gaussian conditional random fields for low-level vision. pages 1–8, 07 2007. 1
- [55] Y. Weiss and W. Freeman. What makes a good model of natural images? pages 1 – 8, 07 2007. 1
- [56] J. Xu and S. Osher. Iterative regularization and nonlinear inverse scale space applied to wavelet-based denoising. *IEEE Transactions on Image Processing*, 16:534–544, 2007. 1
- [57] J. Xu, L. Zhang, and D. Zhang. A trilateral weighted sparse coding scheme for real-world image denoising. In *European Conference on Computer Vision (ECCV)*, pages 21–38, 2018. 2, 7, 8
- [58] J. Xu, L. Zhang, W. Zuo, D. Zhang, and X. Feng. Patch group based nonlocal self-similarity prior learning for image denoising. *IEEE International Conference on Computer Vision (ICCV)*, pages 244–252, 2015. 2
- [59] K. Zhang, W. Zuo, Y. Chen, D. Meng, and L. Zhang. Beyond a Gaussian denoiser: Residual learning of deep CNN for image denoising. *IEEE Transactions on Image Processing*, 26(7):3142–3155, 2017. 1, 3, 7, 8
- [60] K. Zhang, W. Zuo, S. Gu, and L. Zhang. Learning deep cnn denoiser prior for image restoration. *IEEE Conference on Computer Vision and Pattern Recognition (CVPR)*, pages 2808–2817, 2017. 1, 3
- [61] K. Zhang, W. Zuo, and L. Zhang. Ffdnet: Toward a fast and flexible solution for cnn-based image denoising. *IEEE Transactions on Image Processing (TIP)*, 27(9):4608–4622, 2018. 3, 8
- [62] D. Zoran and Y. Weiss. From learning models of natural image patches to whole image restoration. In *IEEE International Conference on Computer Vision (ICCV)*, pages 479–486, 2011. 2, 7